The Astrophysical Journal, 779:158 (14pp), 2013 December 20 doi:10.1088/0004-637X/779/2/158

AN AB INITIO MODEL FOR THE MODULATION OF GALACTIC COSMIC-RAY ELECTRONS

N. E. Engelbrecht and R. A. Burger
Center for Space Research, North-West University, Potchefstroom 2520, South Africa
Received 2013 August 7; accepted 2013 October 23; published 2013 December 3

ABSTRACT

The modulation of galactic cosmic-ray electrons is studied using an ab initio three-dimensional steady state cosmic-ray modulation code in which the effects of turbulence on both the diffusion and drift of these cosmic-rays are treated as self-consistently as possible. A significant refinement is that a recent two-component turbulence transport model is used. This model yields results in reasonable agreement with observations of turbulence quantities throughout the heliosphere. The sensitivity of computed galactic electron intensities to choices of various turbulence parameters pertaining to the dissipation range of the slab turbulence spectrum, and to the choice of model of dynamical turbulence, is demonstrated using diffusion coefficients derived from the quasi-linear and extended nonlinear guiding center theories. Computed electron intensities and latitude gradients are also compared with spacecraft observations.

Key words: cosmic rays – diffusion – turbulence

Online-only material: color figures

1. INTRODUCTION

There has been renewed interest of late in the modulation of cosmic-ray (CR) electrons (see, e.g., Della Torre et al. 2012; Maccione 2013; Potgieter & Nndanganeni 2013). While these studies focus on more traditional aspects of electron modulation, such as the effects of drift (Della Torre et al. 2012) or the local interstellar spectrum (Potgieter & Nndanganeni 2013), the sensitivity of these CRs to the behavior of the low-energy diffusion coefficients (see, e.g., Potgieter 1996; Potgieter & Ferreira 1999) can in principle be taken advantage of to study the effects of turbulence on their modulation. This, however, cannot be done using ad hoc expressions for electron diffusion coefficients. The present study considers the modulation of galactic electrons using the ab initio approach followed by Engelbrecht & Burger (2013), by using the results yielded by the two-component turbulence transport model of Oughton et al. (2011) in the three-dimensional (3D), steady state CR modulation code of Burger et al. (2008) as self-consistently as possible. Parallel mean free paths derived from quasi-linear theory (QLT; Jokipii 1966; Teufel & Schlickeiser 2003) and a perpendicular mean free path derived from the extended nonlinear guiding center (ENLGC) theory of Shalchi (2006) are used. Two electron parallel mean free path expressions, derived for the random sweeping and damping models of dynamical turbulence by Teufel & Schlickeiser (2003), are considered, the former of which having been used previously by Engelbrecht & Burger (2010). At low energies, these mean free-path expressions are sensitive to choices made for turbulence quantities that pertain to the dissipation range of the slab turbulence power spectrum. The effects on computed galactic electron spectra of the dissipation range onset wavenumber and the dissipation range spectral index will be investigated, and will be shown to be so significant that two models for the dissipation range onset wavenumber could be eliminated unambiguously. This study is an extension of that of Engelbrecht & Burger (2010), in that here a turbulence-transport model is used as opposed to the relatively ad hoc expressions used by Engelbrecht & Burger (2010) to describe the spatial dependences of basic turbulence quantities. Moreover, this is a first look at how the two-component turbulence transport model of Oughton et al. (2011) will affect computed galactic electron intensities.

Section 2 introduces the diffusion and drift coefficients used in this study, while Section 3 provides a brief introduction to the various dissipation range turbulence quantities relevant to this study. Section 4 characterizes the low-energy mean free path expressions as functions of the dissipation range turbulence quantities, and Section 5 considers their effect on computed galactic electron intensity spectra and latitude gradients. A summary and conclusions are given in Section 6.

2. DIFFUSION AND DRIFT COEFFICIENTS

The power spectra of turbulent fluctuations in the heliospheric magnetic field (HMF) are key inputs for the various theories used to describe the diffusion of CRs in the heliosphere (see, e.g., Bieber et al. 1994; Shalchi 2009), and turbulence has been shown to play a role in the reduction of CR gradient and curvature drifts (see, e.g., Minnie et al. 2007b). In this study, the turbulence quantities of which these power spectra are functions, such as the magnetic variances, are modeled using the results yielded by the two-component turbulence transport model of Oughton et al. (2011). This model is solved following the same approach discussed in detail by Engelbrecht (2013) and also used by Engelbrecht & Burger (2013), using the same boundary conditions as these authors, which were chosen so that the results yielded would be in fair to good agreement with extant spacecraft observations of turbulence quantities throughout the heliosphere. For more detail as to turbulence transport, the interested reader is invited to consult, e.g., Tu & Marsch (1993), Oughton et al. (2006), and Breech et al. (2008).

The present study uses two different parallel mean free path expressions based on those derived from the QLT of Jokipii (1966) by Teufel & Schlickeiser (2003), under the assumption of composite turbulence (Bieber et al. 1994). Teufel & Schlickeiser (2003) use the following slab modal spectrum, based on the

results of Bieber et al. (1994):

$$G^{\rm slab}(k_\parallel) = \begin{cases} g_o k_m^{-s},\ |k_\parallel| \leqslant k_m; \\ g_o |k_\parallel|^{-s},\ k_m \leqslant |k_\parallel| \leqslant k_d; \\ g_1 |k_\parallel|^{-p},\ |k_\parallel| \geqslant k_d. \end{cases} \quad (1)$$

The above spectrum forms part of a total turbulence modal spectrum defined in this study such that $G(\mathbf{k}) = G^{\rm slab}(k_\parallel)\delta(k_\perp) + G^{\rm 2D}(k_\perp)\delta(k_\parallel)$, where $G^{\rm 2D}(k_\perp)$ denotes a two-dimensional (2D) modal spectrum. The subscripts "$\parallel$" and "$\perp$" denote directions parallel and perpendicular to the background magnetic field, and that if the parallel direction is denoted arbitrarily by 1, then $k_\parallel = k_1$ and $k_\perp^2 = k_2^2 + k_3^2$. In Equation (1), $k_m = 1/\lambda_{sl}$ is the parallel wavenumber associated with the onset of the inertial range and k_d is the wavenumber associated with the onset of the dissipation range. The spectral index in the dissipation range is denoted by s, and is here assumed to have the Kolmogorov value of 5/3, while p denotes the spectral index in the dissipation range. The spectral index of the dissipation range is expected to be steeper than that of the inertial range, and dependent on the processes driving the ultimate dissipation of energy (Smith et al. 1990). In this study, this index is confined to the range $p = 2.61 \pm 0.96$, following the observations reported by Smith et al. (2006). Furthermore,

$$g_o = \left[s + \frac{s-p}{p-1} \left(\frac{k_m}{k_d} \right)^{s-1} \right]^{-1} \frac{\delta B_{sl}^2 k_m^{s-1} (s-1)}{8\pi} \quad (2)$$

and $g_1 = g_0 k_d^{p-s}$, with δB_{sl}^2 denoting the slab variance.

Teufel & Schlickeiser (2003) derive piecewise continuous expressions using Equation (1) for both the random sweeping and damping models for dynamical turbulence. If the dynamical character of turbulence is taken into account, the scattering rate at and near 90° pitch angle is seen to be governed by resonance with the Eulerian frequency spectrum. A mass dependence in the scattering mean free path occurs because the resonance is at the particle gyrofrequency (see Bieber et al. 1994). Engelbrecht & Burger (2010) use a continuous parallel mean free path expression constructed from the random sweeping results of Teufel & Schlickeiser (2003), given by

$$\lambda_\parallel = \frac{3s}{\sqrt{\pi}(s-1)} \frac{R^2}{k_{\rm min}} \left(\frac{B_o}{\delta B_{\rm slab}} \right)^2 \cdot \left[\frac{1}{4\sqrt{\pi}} + \left(\frac{1}{\Gamma(p/2)} + \frac{1}{\sqrt{\pi}(p-2)} \right) \frac{b^{p-2}}{Q^{p-s} R^s} + \frac{2}{\sqrt{\pi}(2-s)(4-s)} \frac{1}{R^s} \right]. \quad (3)$$

Another electron parallel mean free path expression can be similarly constructed for the damping model results of Teufel & Schlickeiser (2003), and is given by (Engelbrecht 2013)

$$\lambda_\parallel = \frac{3s}{\sqrt{\pi}(s-1)} \frac{R^2}{k_{\rm min}} \left(\frac{B_o}{\delta B_{\rm slab}} \right)^2 \cdot \left[\frac{1}{4\sqrt{\pi}} {}_2F_1 \left(1, \frac{1}{p-1}, \frac{p}{p-1}; -\frac{\pi a}{f_1} Q^{p-2} \right) \times \frac{\sqrt{\pi} a}{f_1 R^s Q^{p-s}} + \frac{2}{\sqrt{\pi}(2-s)(4-s)} \frac{1}{R^s} \right], \quad (4)$$

where

$$a = \frac{v}{\alpha_d V_A},$$
$$b = a/2,$$
$$R = R_L k_{\rm min},$$
$$Q = R_L k_d,$$
$$f_1 = \frac{2}{p-2} + \frac{2}{2-s}, \quad (5)$$

with v the particle speed, $R_L = P/B_o$ denoting the maximal Larmor radius, and $P = pc/|q_c|$ the particle rigidity, and V_A the Alfén speed, following the notation of Teufel & Schlickeiser (2003). The parameter $\alpha_d \in [0, 1]$ adjusts dynamical effects, such that a value of zero corresponds to the magnetostatic limit, while a value of unity assumes that the underlying turbulence is strongly dynamical (Bieber et al. 1994). In the above, Γ denotes the Gamma function, and ${}_2F_1$ the Gauss hypergeometric function.

These QLT-based parallel mean free path expressions display a rigidity dependence at the lowest rigidities in reasonable agreement with observations of this quantity. Comparison of observed proton and electron mean free paths led Bieber et al. (1994) to conclude that below 25 MV, the Palmer (1982) consensus range pertains to electrons only, being applicable to protons only above that rigidity. Bieber et al. (1994) also find significant variations in magnitude of the observed mean free paths on an event-by-event basis. When individual events are considered, Bieber et al. (1994) report that for protons, the $P^{1/3}$ rigidity dependence of the magnetostatic slab quasi-linear theoretical result appears to be accurate, although these theoretical mean free paths remain well below all observed values for a purely slab model of turbulence. The electron mean free paths, however, appeared to behave in a fundamentally different manner, appearing to be rigidity-independent at the rigidities considered, so much so that Bieber et al. (1994) report that the electron mean free paths at ~1.4 MV are essentially the same as those for protons at ~187 MV. This essentially rigidity-independent behavior of low-energy electron mean free paths was also reported for 1–10 MV electrons by Dröge (1994). Dröge (2000) and Dröge (2003), in detailed subsequent studies of electron and proton mean free paths acquired via fits of solar energetic particle events using a focused transport model, report observations of the rigidity dependences of these mean free paths in agreement with those of Bieber et al. (1994), displaying a low-energy electron mean free path fundamentally different to that of the protons. The agreement also extends to the large event-to-event variations in magnitude observed for mean free paths. It is interesting to note, however, that although the magnitude of the mean free path changes with different events in these studies, the rigidity dependences remain essentially the same. The observed increase in the electron parallel mean free path at low energies is a natural outcome of the dynamical nature of turbulence as discussed by Bieber et al. (1994). Furthermore, these authors showed that a composite of slab and 2D turbulence can solve the magnitude problem of parallel mean free paths referred to earlier. The choice of QLT-based mean free paths in this study is also motivated by the reasonable agreement of the predictions of this theory with numerical simulations of the parallel diffusion coefficient for relatively low levels of composite turbulence (Minnie et al. 2007a).

The perpendicular mean free path expression used in this study is that of Engelbrecht (2013; see also Engelbrecht & Burger 2013), derived using the ENLGC theory of Shalchi (2006), which, in turn, is based on the nonlinear guiding center (NLGC) theory of Matthaeus et al. (2003). A review of this and other scattering theories is given by, e.g., Shalchi (2009). This particular choice of scattering theory is motivated by the fact that the predictions of the NLGC theories agree well with numerical simulations over a broad range of rigidities and turbulence levels (Shalchi 2006; Minnie et al. 2007a) as well as with observations at Earth. Engelbrecht & Burger (2013) assume a 2D omnidirectional spectrum following Matthaeus et al. (2007), with a Kolmogorov inertial range, a flat energy range, and an "outer range" that decreases steeply at the lowest wavenumbers. The 2D modal spectrum corresponding to an omnidirectional spectrum of this form can be expressed as

$$G^{2D}(k_\perp) = g_2 \begin{cases} (\lambda_{\rm out} k_\perp)^q, & |k_\perp| < \lambda_{\rm out}^{-1}; \\ 1, & \lambda_{\rm out}^{-1} \leqslant |k_\perp| < \lambda_{\rm 2D}^{-1}; \\ (\lambda_{\rm 2D} k_\perp)^{-\nu}, & |k_\perp| \geqslant \lambda_{\rm 2D}^{-1}, \end{cases} \tag{6}$$

where $g_2 = (C_o \lambda_{\rm 2D} \delta B_{\rm 2D}^2)/(2\pi k_\perp)$, and

$$C_0 = \left[\left(1 - \frac{q}{1+q} \left(\frac{\lambda_{\rm 2D}}{\lambda_{\rm out}} \right) + \frac{1}{\nu - 1} \right) \right]^{-1} \tag{7}$$

with $\nu = 5/3$ the spectral index in the inertial range and q the spectral index in the "outer range," which, based on physical considerations argued by Matthaeus et al. (2007), is set to 3 in this study. The lengthscale $\lambda_{\rm 2D}$ denotes the 2D bendover scale, corresponding to the wavenumber at which the inertial range commences, while $\lambda_{\rm out}$ denotes the 2D outerscale, which, in turn, corresponds to the wavenumber at which the energy range commences, such that $\lambda_{\rm out} > \lambda_{\rm 2D}$. No observations currently exist for the 2D outerscale, and it is here assumed that $\lambda_{\rm out} = 12.5\lambda_{c,\rm 2D}$, with $\lambda_{c,\rm 2D}$ the 2D correlation scale (see, e.g., Bruno & Carbone 2005; Matthaeus et al. 2007; Matthaeus & Velli 2011). The motivation behind this simple dependence is that this choice of 2D outerscale led to reasonably good agreement of modeled galactic proton and antiproton CR intensities with spacecraft observations (Engelbrecht & Burger 2013). Using Equation (6), Engelbrecht & Burger (2013) follow the approach outlined by Shalchi et al. (2004a), but using the ENLGC theory of Shalchi (2006), to find that

$$\lambda_\perp = \frac{2a_n^2}{B_o^2} \frac{C_0 \lambda_{\rm 2D} \delta B_{\rm 2D}^2}{\lambda_\perp} [h_{\perp,1} + h_{\perp,2} + h_{\perp,3}], \tag{8}$$

with

$$h_{\perp,1} = \frac{\lambda_\parallel \lambda_\perp}{(1+q)\lambda_{\rm out}} {}_2F_1 \left(1, \frac{1+q}{2}, \frac{3+q}{2}; -x^{-2} \right),$$

$$h_{\perp,2} = \sqrt{3\lambda_\parallel \lambda_\perp} \left[\arctan(x) - \arctan(y) \right],$$

$$h_{\perp,3} = \frac{3\lambda_{\rm 2D}}{(1+\nu)} {}_2F_1 \left(1, \frac{1+\nu}{2}, \frac{3+\nu}{2}; -y^2 \right),$$

where

$$x = \frac{\sqrt{3}\lambda_{\rm out}}{\sqrt{\lambda_\parallel \lambda_\perp}},$$

$$y = \frac{\sqrt{3}\lambda_{\rm 2D}}{\sqrt{\lambda_\parallel \lambda_\perp}},$$

with a_n^2 a constant set to a value of 1/3, following Matthaeus et al. (2003). The above expressions are evaluated numerically in this study. Here, as in Engelbrecht & Burger (2013), the assumption of axisymmetric perpendicular diffusion is made. Note that Equation (8) is derived, as a first approach, under the assumption of magnetostatic fluctuations. Dynamical effects, when taken into account in both the quasi-linear and NLGC theories (see, e.g., Shalchi & Schlickeiser 2004; Shalchi et al. 2004b, 2006) lead to considerably more complicated expressions for the perpendicular mean free path, which will be a topic for future study. The perpendicular mean free path used in this study is qualitatively similar to that presented by Pei et al. (2010a), but differs due to a different form for the 2D modal spectrum used by those authors. Pei et al. (2010a) also use a different turbulence transport model to provide inputs for their 2D spectrum, the single component model of Breech et al. (2008).

The effects of turbulence on drifts are modeled following the approach of Engelbrecht (2013) and Engelbrecht & Burger (2013), who use the drift coefficient proposed by Burger & Visser (2010). From Bieber & Matthaeus (1997),

$$\kappa_A = \frac{v}{3} R_L \frac{\Omega^2 \tau^2}{1 + \Omega^2 \tau^2}, \tag{9}$$

where Ω is the particle gyrofrequency and τ is a decorrelation rate. We use a parameterized form for $\Omega\tau$ proposed by Burger & Visser (2010), which was constructed so as to yield a drift coefficient in agreement with numerical simulations performed by Minnie et al. (2007b)

$$\Omega\tau = \frac{11}{3} \frac{\sqrt{R_L/\lambda_{c,s}}}{(D_\perp/\lambda_{c,s})^g}, \tag{10}$$

where $g = 0.3 \log(R_L/\lambda_{c,s}) + 1.0$, and $D_\perp$ is the field line random walk diffusion coefficient (Matthaeus et al. 1995)

$$D_\perp = \frac{1}{2} \left(D_{sl} + \sqrt{D_{sl}^2 + 4D_{\rm 2D}^2} \right),$$

$$D_{sl} = \frac{1}{2} \frac{\delta B_{sl}^2}{B_o^2} \lambda_{c,s},$$

$$D_{\rm 2D} = \frac{\sqrt{\delta B_{\rm 2D}^2/2}}{B_o} \lambda_u.$$

The field line random walk coefficient is, in turn, a function of the 2D ultrascale λ_u (see, e.g., Matthaeus et al. 1999, 2007), which, for the 2D spectrum given by Equation (6), is calculated by Engelbrecht & Burger (2013) to be

$$\lambda_u = \left[C_0 \lambda_{\rm 2D} \left(\frac{q}{q-1} \lambda_{\rm out} - \frac{\nu}{1+\nu} \lambda_{\rm 2D} \right) \right]^{\frac{1}{2}}, \tag{11}$$

following the approach of Matthaeus et al. (2007). The various turbulence quantities that this drift coefficient requires as inputs are also acquired from the results of the Oughton et al. (2011) turbulence transport model.

3. DISSIPATION RANGE TURBULENCE QUANTITIES

The electron parallel mean free path expressions discussed above are very sensitive to the choice of dissipation range turbulence quantities used. These quantities cannot be acquired from the Oughton et al. (2011) turbulence transport model, and

Table 1
Parameters and χ^2 Values of Regressions Applied by Leamon et al. (2000) to Observed Breakpoint Frequencies

X	a_L	b_L	χ^2
$2\pi\Omega_{ci}$	0.200	1.760	2.93
	0	3.190	3.88
$k_{ii}V_{sw}$	0.152	0.451	2.66
	0	0.686	3.07

Notes. Fits are of the form $\nu_{bp} = a_L + b_L X/2\pi$, with $a_L = 0$ for the fit-through-origin models.

as such need to be modeled independently. This section provides a brief background and motivation for the choices and models for these quantities used in this study. For more detail, see, e.g., Carbone (2012).

3.1. The Dissipation Range Onset Lengthscale

Only two of the three models for the onset wavenumber of the dissipation range suggested by Leamon et al. (2000), those that according to these authors give the best agreement with data, will be considered here. Those are where this wavenumber is either a function of the proton gyrofrequency (Goldstein et al. 1994; Leamon et al. 1998b),

$$\Omega_{ci} = |q_c|B_o/m, \tag{12}$$

where $|q_c|$ denotes charge and m mass; or of the local ion inertial scale,

$$\rho_{ii} = \frac{V_A}{\Omega_{ci}}. \tag{13}$$

Leamon et al. (2000) argue that, should the latter be the case, the dissipation range would commence at the ion inertial scale because of the formation of local current sheet structures perpendicular to the mean magnetic field. These authors then compare the models to dissipation range onset wavenumbers they acquired from *WIND* data (the details of which analysis to be found in Leamon et al. 1998a), applying best-fit and fit-through-origin linear regressions to these observations, such that the dissipation range onset wavenumber can be expressed by

$$k_D = \frac{2\pi}{V_{sw}}(a_L + b_L\Omega_{ci}), \tag{14}$$

or

$$k_D = \frac{2\pi}{V_{sw}}\left(a_L + \frac{b_L}{2\pi}k_{ii}V_{sw}\right), \tag{15}$$

depending on the model chosen, with

$$k_{ii} = \frac{2\pi\sin\Psi}{\rho_{ii}} = \frac{2\pi\Omega_{ci}\sin\Psi}{V_A}, \tag{16}$$

and Ψ denoting the HMF winding angle. The regression constants a_L and b_L in the above equations are listed in Table 1, given in terms of the dissipation range breakpoint frequencies associated with each model. As it turns out, the two ion inertial scale models yield dissipation range breakpoint frequencies at 1 AU, listed in Table 2, closest to that of ~0.44 Hz observed by Leamon et al. (1998b), while the proton gyrofrequency models are in better agreement with the values of ~0.3 Hz reported by Hamilton et al. (2008) and of ~0.2 Hz given by Smith et al. (2012). However, the χ^2 value for the best-fit ion inertial scale regression reported by Leamon et al. (2000) seems to imply that this model is most apt to describe the onset of the dissipation range, at least at 1 AU.

Table 2
Values in Hz for the Breakpoint Frequency ν_{bp} at 1 AU Predicted by the Various Models and Fits of Leamon et al. (2000)

$k_D(k_{ii})$ Best Fit	$k_D(k_{ii})$ Through Origin	Ω_{ci} Best Fit	Ω_{ci} Through Origin
0.456	0.452	0.298	0.178

The present study, similar to that of Engelbrecht & Burger (2010), aims to model the global behavior of k_D throughout the heliosphere, using the expressions proposed by Leamon et al. (2000) for conditions at Earth, given by Equations (14) and (15). These models are derived for observations at Earth, and as such their use is potentially a risky endeavor, in that for varying conditions (turbulent and otherwise) throughout the heliosphere, such an extrapolation may lead to unphysical modeled spectra, which may, in turn, lead to unrealistic derived mean free paths. The present subsection, then, also aims to characterize the models for k_D discussed above at various regions in the heliosphere, chosen so as to both highlight the spatial dependences of the various models for this quantity, as well as to point out potentially unphysical scenarios arising from this extrapolation.

Figure 1, from Engelbrecht (2013), illustrates the values yielded by the Leamon et al. (2000) best-fit and fit-through-origin ion inertial scale and proton gyrofrequency models for the dissipation range breakpoint wavenumber as functions of radial distance in the ecliptic plane, and as functions of colatitude at 1 AU and 100 AU, acquired by assuming a 100 AU heliosphere, a Parker (1958) HMF and a radially constant solar-wind speed profile that varies from 400 km s^{-1} to 800 km s^{-1} from ecliptic to polar latitudes (see, e.g., McComas et al. 2000). Also shown in Figure 1 are values of the inertial range breakpoint wavenumber $k_{\min}$ used in the present study, calculated from the slab correlation scale yielded by the Oughton et al. (2011) two-component turbulence transport model. This is done so as to test whether or not $k_{\min}$ remains smaller than k_D throughout the heliosphere, a condition that ensures a well-defined inertial range on the modeled slab spectrum discussed earlier. If this condition is not met, it can lead to problematic scenarios involving the parallel mean free paths used in the present study, as these were derived assuming a well-defined inertial range.

The top panel of Figure 1 shows a clear difference between the best-fit and fit-through-origin models for k_D, with the fit-through-origin values, for both the ion inertial and proton-gyrofrequency models, decreasing monotonically with increasing radial distance through most of the heliosphere, as opposed to the relatively constant radial profiles displayed by the best-fit models. The latter behavior is due to the additional constant factor a_L. Furthermore, both best-fit models yield very similar results in the outer heliosphere, with the ion inertial scale fit-through-origin model yielding results higher than those of the proton gyrofrequency fit-through-origin model. When compared with $k_{\min}$, all models yield results well above this quantity, thereby satisfying the condition that $k_D > k_{\min}$.

When considered as functions of colatitude in the bottom panels of Figure 1, all models yield results larger in the ecliptic than over the poles. The best-fit models again yield similar results, and for a large range of colatitudes about the ecliptic plane, the ordering of values for k_D yielded by these models remains the same as that displayed in the top panel of Figure 1.

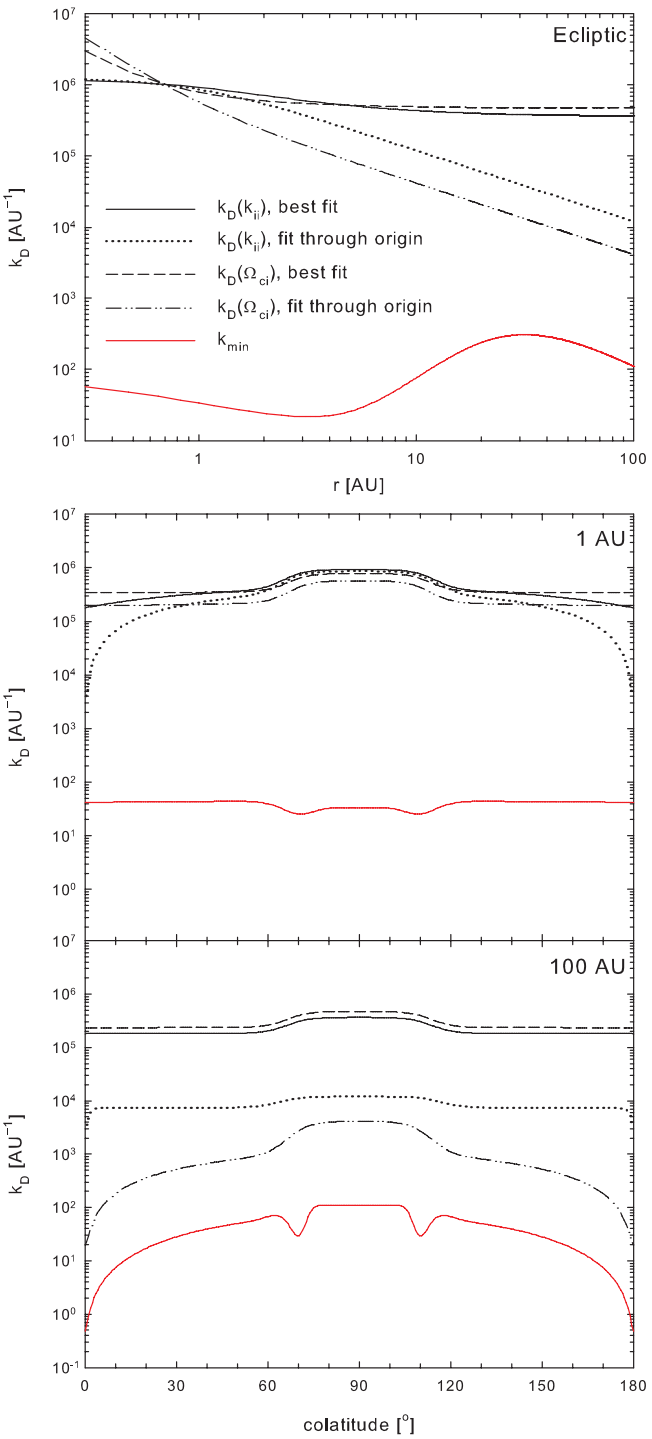

Figure 1. Various 1 AU Leamon et al. (2000) models used in the present study for the dissipation range onset wavenumber k_D, extrapolated as a function of radial distance in the ecliptic plane (top panel), and as functions of colatitude at 1 AU (middle panel) and 100 AU (bottom panel), from Engelbrecht (2013). The inertial range onset wavenumber $k_{\min}$, calculated from results yielded by the two-component turbulence transport model of Oughton et al. (2011), is also shown (red lines).

(A color version of this figure is available in the online journal.)

Over the poles, however, things become more complicated for both radial distances considered. In this region, the proton gyrofrequency becomes quite small, and directly over the poles, the sine of the heliospheric winding angle becomes zero. The best-fit values remain relatively unaffected by this, due again to the constant factor a_L in Equations (14) and (15). The fit-through-origin gyrofrequency model, however, yields very small values for k_D, and although this is not clear because of the logarithmic scale of the figure, the fit-through-origin ion inertial scale model yields a zero result for this quantity directly over the poles. However, even though the fit-through-origin proton-gyrofrequency model yields very small values for k_D over the poles, these values remain larger than the illustrated inertial range breakpoint wavenumber, as do those yielded by both best-fit models. Because of the fit-through-origin ion inertial scale model yielding zero values for k_D over the poles, this model will not be considered in subsequent modulation studies presented here, although an alternative model for the HMF can be used to avoid this issue (see, e.g., Burger et al. 2008; Engelbrecht & Burger 2010).

3.2. The Dissipation Range Spectral Index

The spectral index of the dissipation range is expected to be steeper than that of the inertial range, and dependent on the processes driving the ultimate dissipation of energy (Smith et al. 1990). From magnetohydrodynamic (MHD) theory, the spectral index of the dissipation range is expected to be equal to -3 or steeper, as any other value would imply that the mean square of the curl of the total magnetic field would be divergent (Bieber et al. 1988; Smith et al. 1990; Bieber et al. 1994). The solar wind, however, is a weakly collisional plasma, and thus the dissipation of energy below scales at which MHD theory no longer applies must of necessity be described by kinetic (see, e.g., Marsch 2006) or gyrokinetic theories (see, e.g., Howes et al. 2008). The range of indices reported by Smith et al. (2006) and Hamilton et al. (2008, who find values for this quantity similar to those reported by Smith et al. 2006) are difficult to reconcile with theory. Because the solar wind is a weakly collisional plasma, descriptions of the behavior of the turbulence in the dissipation range must out of necessity be kinetic. Various mechanisms have been proposed as to how dissipation occurs: Stawicki et al. (2001) proposed dispersion due to the action of whistler waves, while Leamon et al. (2000) argue that the effects of Landau damping could also play a role. Ion cyclotron damping has also been proposed as a possible mechanism for turbulent dissipation (see, e.g., Goldstein et al. 1994). If dissipation were to commence at wavenumbers corresponding to the ion inertial scale (Leamon et al. 2000), representing as it does the scale below which the fluid approximation breaks down (Smith et al. 2006; Alexandrova et al. 2008), the fact that the spectral index of the dissipation range depends on the rate at which energy cascades through the inertial range, as reported by Smith et al. (2006), should also play a role. Smith et al. (2006) conclude that if this were the case, and the lengthscale at which the dissipation range begins does not change, the form of the spectrum will adjust accordingly. It is intriguing to note, however, that Alexandrova et al. (2008) find evidence of a further inertial range beyond the aforementioned dissipation range onset lengthscale. As noted above, the range of values for p considered in this study will remain within the uncertainty of the $p = 2.61 \pm 0.96$ range reported for this quantity by Smith et al. (2006).

4. CHARACTERIZING THE PARALLEL MEAN FREE PATH: LOW-RIGIDITY ELECTRON MEAN FREE PATHS

The present section aims to briefly consider the dependence of low-energy electron parallel mean free paths, for both the random sweeping and damping models of dynamical turbulence,

on the dissipation range breakpoint wavenumber and spectral index. Note that for the mean free paths considered here, turbulence quantities such as the variance and correlation scale yielded by the two-component Oughton et al. (2011) turbulence-transport model for solar minimum conditions have been used. The use of this turbulence transport model leads to considerably more complicated spatial dependences for these quantities than for those considered in most previous studies of this nature, such as that of Engelbrecht & Burger (2010). Throughout what follows, the Parker (1958) model for the HMF is used, as is a latitude-dependent solar wind speed modeled using a hyperbolic tangent function that assumes a value of 400 km s^{-1} in the ecliptic and 800 km s^{-1} over the poles, and a Kolmogorov 5/3 value is here assumed for the spectral index of the inertial range s.

The low-energy electron mean free paths, as described by Equations (3) and (4) for the random sweeping and damping models of dynamical turbulence, respectively, are shown as functions of rigidity at 1 AU and 100 AU for the various Leamon et al. (2000) models for k_D in Figure 2. At high rigidities, the mean free paths for the two models both show a clear $P^{1/3}$ rigidity dependence. The differences at low rigidities are quite remarkable, and reflect the results of Teufel & Schlickeiser (2003), where the damping electron mean free path is considerably smaller than that yielded by the random sweeping model. Both electron mean free paths overshoot the Palmer consensus range at all rigidities considered, a consequence of the choice of solar minimum turbulence quantities made in the present study. However, the mean free paths shown here fall in the upper range of the various observations from Bieber et al. (1994 and references therein) shown in the top panel of Figure 2.

The random sweeping parallel mean free paths for larger values of k_D are lower at small rigidities (see Figure 1), reflecting the k_D^{s-p} dependence reported by Engelbrecht & Burger (2010). This behavior can also be seen in the damping turbulence mean free paths, although the dependence on the magnitude of k_D is not as strong as in the random sweeping case. Mean free paths acquired using the best-fit ion inertial and proton gyrofrequency models for k_D tend to be very similar, because these models yield very similar values for this quantity, as can be seen in Figure 1. Overall, k_D has a relatively moderate effect on the electron parallel mean free paths at 1 AU, in contrast with their behavior at 100 AU, where the parallel mean free paths acquired using both best-fit models for the dissipation range breakpoint theory are considerably smaller than those acquired assuming the fit-through-origin gyrofrequency model. This is a consequence of the large decrease in HMF magnitude with increased heliocentric radial distance having a strong, lowering effect on the fit-through-origin gyrofrequency model. This is an effect that is masked in the best-fit models due to the non-zero values of the constant a_L in Equations (14) and (15). While the larger random sweeping parallel mean free paths for the best-fit k_D models flatten out at the lowest rigidities shown, the lower damping turbulence mean free paths for these models seem not to show the effects of a dissipation range at all, displaying only the $P^{1/3}$ and P^2 rigidity dependences one would expect of proton parallel mean free paths. This again remains a consequence of the larger values for k_D yielded by these models, which act so as to reduce the significance of the dissipation range on the slab spectrum, thereby reducing the action of the dissipation range-dependent terms in Equations (3) and (4) for the mean free paths acquired from both models of dynamical turbulence.

As functions of colatitude, shown in Figure 3, the 0.01 GV electron mean free paths display the same order of increase

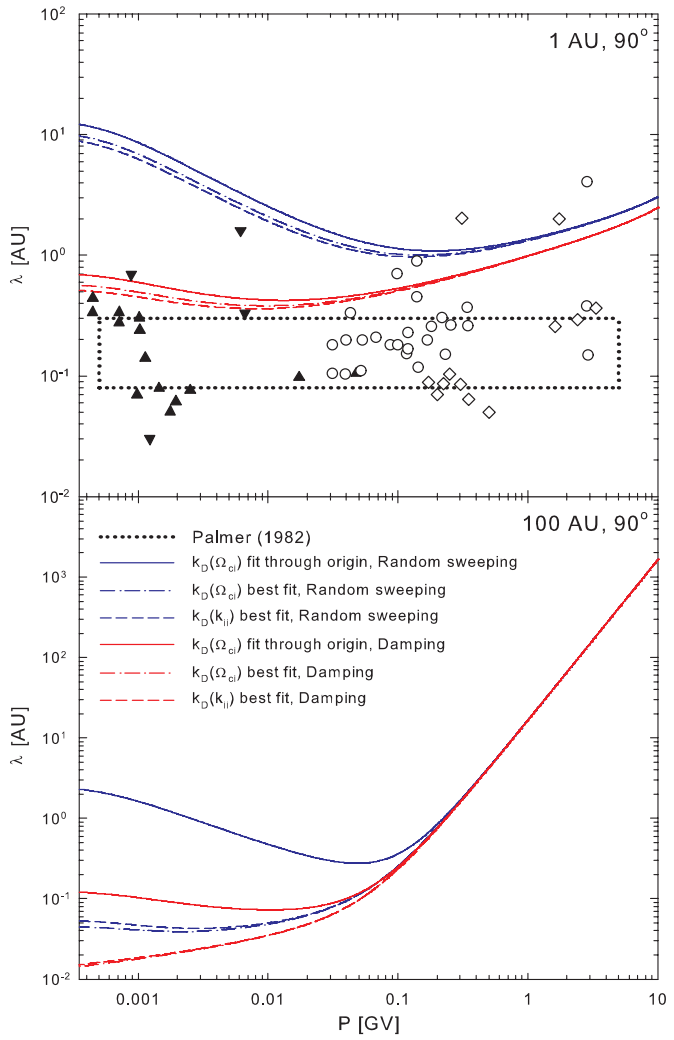

Figure 2. Random sweeping and damping turbulence electron parallel mean free paths used in the present study as functions of rigidity at 1 AU (top panel) and 100 AU (bottom panel) in the ecliptic plane for various models for the dissipation range breakpoint wavenumber proposed by Leamon et al. (2000), from Engelbrecht (2013). The quantities Ω_{ci} and k_{ii} in brackets denote dissipation breakpoint wavenumbers based on the proton gyrofrequency and ion inertial scale, respectively. Also shown at 1 AU is the Palmer (1982) consensus range (denoted by the dotted rectangle) and various parallel mean free path observations (Bieber et al. 1994 and references therein), where filled symbols denote observations of electron parallel mean free paths, while open symbols denote observations of proton parallel mean free paths.

(A color version of this figure is available in the online journal.)

with smaller corresponding values for k_D as discussed above, for the same reasons. In general, the latitudinal behavior of these mean free paths is in qualitative agreement with that reported by Erdös & Balogh (2005). As functions of colatitude, all parallel mean free paths shown here are quite sensitive to the colatitudinal behavior of the turbulence quantities yielded by the Oughton et al. (2011) model (see Engelbrecht & Burger 2013). All mean free paths shown at 1 AU are larger in the ecliptic plane, with its lower variance values, than toward the poles, displaying slight "dips" at colatitudes corresponding to the larger variances associated with regions of greater modeled shear effects. At colatitudes smaller (or larger, depending on which hemisphere is considered) than these regions, the proton parallel mean free paths for both dynamical turbulence models become almost constant as functions of colatitude, reflecting the behavior of the modeled slab variance and correlation scales,

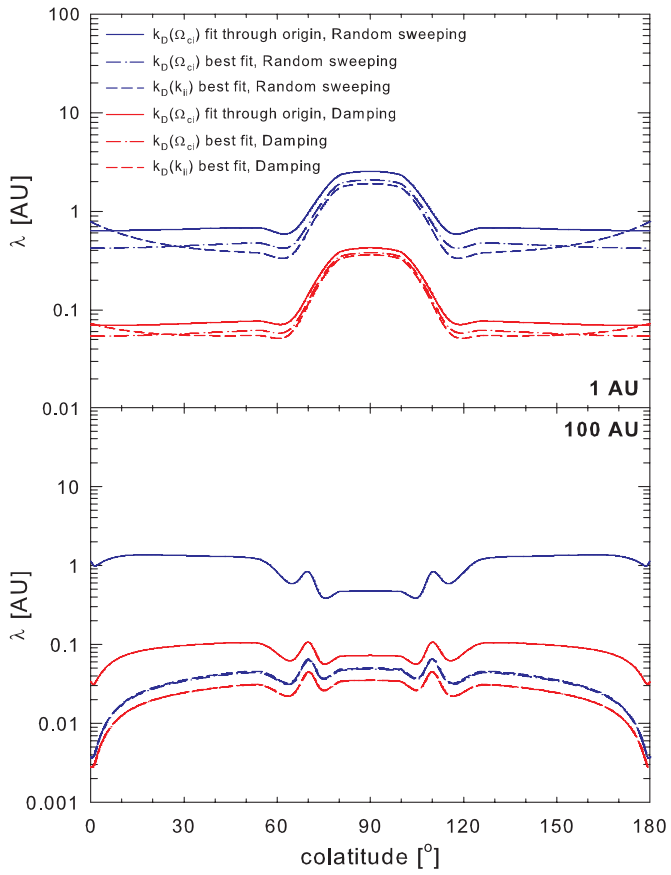

Figure 3. Random sweeping and damping turbulence 0.01 GV electron parallel mean free paths used in the present study as functions of colatitude at 1 AU (top panel) and 100 AU (bottom panel) for various models for the dissipation range breakpoint wavenumber proposed by Leamon et al. (2000), from Engelbrecht (2013). The quantities Ω_{ci} and k_{ii} in brackets denote dissipation breakpoint wavenumbers based on the proton gyrofrequency and ion inertial scale, respectively.

(A color version of this figure is available in the online journal.)

which, at this radial distance, remain relatively constant as functions of colatitude. The great sensitivity of these mean free path expressions to the behavior of the variances in particular is due to their stronger dependence on this quantity, since $\lambda_{\parallel} \sim (\delta B_{\rm slab})^{-2}$. The damping turbulence mean free paths are consistently smaller than their random sweeping equivalents, at both 1 AU and 100 AU. The mean free paths yielded by the best-fit models for the dissipation range breakpoint wavenumber are very similar over most colatitudes, due to the similarity of the values of k_D yielded by these models. Approaching the heliospheric poles at 1 AU, however, the best-fit ion inertial scale model mean free path increases somewhat. This is due to the smaller values for k_D that this model yields in this region, shown in Figure 1, as a consequence of the increased Alfvén speed over the poles. At 100 AU, the mean free paths for all models for k_D show a marked decrease toward the poles, with the steepest decrease corresponding to the largest values for k_D. For completeness, the radial dependences of these mean free paths are also shown in Figure 4. The choice of k_D affects the magnitude of the electron mean free paths, for both random sweeping and damping models of dynamical turbulence, in exactly the same way as in the previous cases, with larger values of k_D yielding smaller parallel mean free paths. The best-fit models yield very similar radial dependences, since these quantities are both approximately constant in the outer heliosphere as shown in Figure 1, and yield values very close to one another for the dissipation range breakpoint wavenumber. In the outer heliosphere, the markedly different radial dependence seen in Figure 1 of the fit-through-origin proton gyrofrequency model for k_D does not translate to a vastly different radial dependence for the parallel mean free path acquired from it, when compared with those of the best-fit models. Only in the very inner heliosphere, within 1 AU, do these models appear to have a significant effect on the radial dependence of these low-energy electron parallel mean free paths. In Figure 4, it can again clearly be seen that the damping turbulence mean free paths are not as strongly dependent on k_D as are the random sweeping mean free paths, as the difference between the best-fit and fit-through-origin damping turbulence mean free paths is considerably less than for the random sweeping mean free paths.

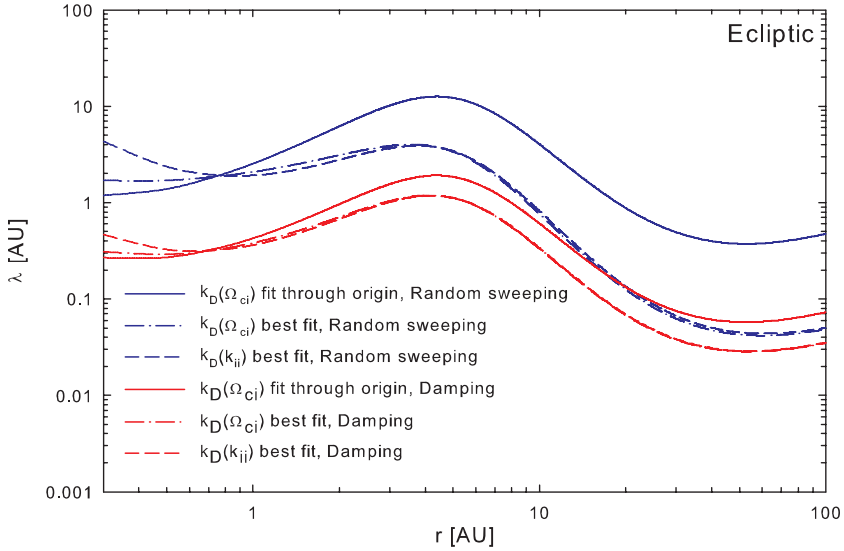

Figure 4. Random sweeping and damping turbulence 0.01 GV electron parallel mean free paths used in the present study as functions of radial distance in the ecliptic plane for various models for the dissipation range breakpoint wavenumber proposed by Leamon et al. (2000), from Engelbrecht (2013).

(A color version of this figure is available in the online journal.)

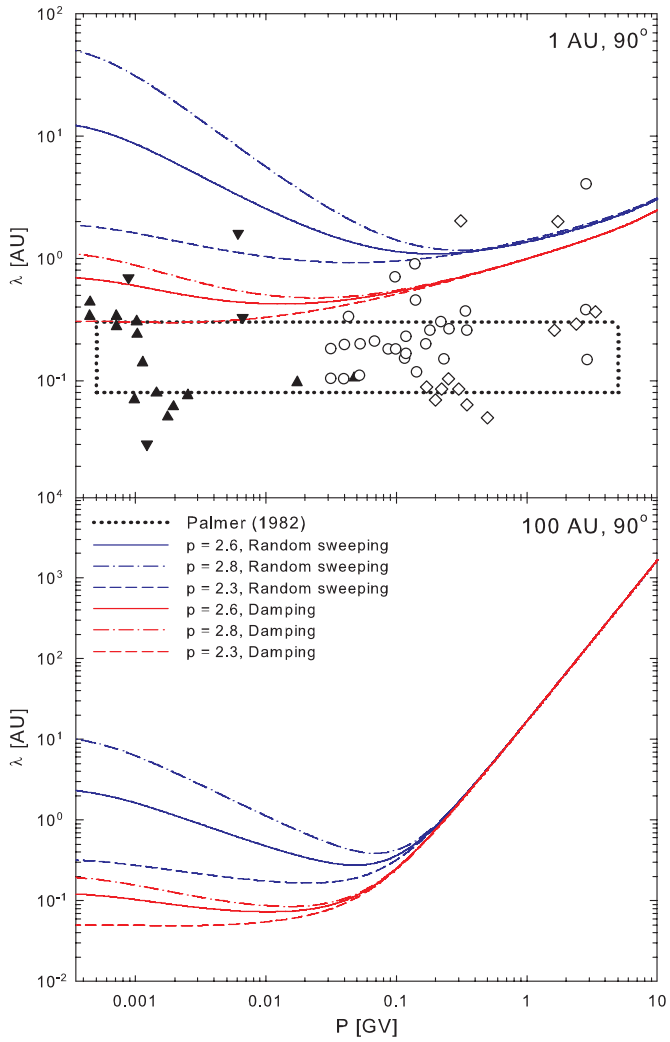

Figure 5. Random sweeping and damping turbulence electron parallel mean free paths used in the present study, as functions of rigidity at 1 AU (top panel) and 100 AU (bottom panel) in the ecliptic plane for various values of the dissipation range spectral index within the range of values reported by Smith et al. (2006), from Engelbrecht (2013). Also shown at 1 AU is the Palmer (1982) consensus range (denoted by the dotted rectangle) and various parallel mean free path observations (Bieber et al. 1994 and references therein), where filled symbols denote observations of electron parallel mean free paths, while open symbols denote observations of proton parallel mean free paths. Note that the mean free paths shown are acquired using the fit-through-origin proton gyrofrequency model for the dissipation range breakpoint wavenumber.

(A color version of this figure is available in the online journal.)

Low-energy electron parallel mean free paths are expected to increase in magnitude if the dissipation range spectral index increases, as a result of the associated decrease in the level of turbulence at high wavenumbers. This is shown in Figure 5, where electron mean free paths, for both the damping and random sweeping models of dynamical turbulence, are shown for various values of p at 1 AU and at 100 AU in the ecliptic. Note that for these mean free paths the fit-through-origin proton gyrofrequency model for k_D was used. The reasons for this choice will be made clear in what follows. Both random sweeping and damping electron mean free paths increase when p is increased, and vice versa. For the values of p considered here, the damping turbulence mean free paths come close to the Palmer consensus range at 1 AU, with the $p = 2.3$ case actually touching on the upper part of this range, but still remain mostly above it. The random sweeping mean free paths remain much larger than the Palmer consensus range, even for the smallest value of p considered. The mean free paths shown in Figure 5, however, still fall in the upper range of the various observations from Bieber et al. (1994 and references therein) shown in the top panel of that figure. As for the case of the dissipation range breakpoint wavenumber, the damping turbulence mean free paths appear less sensitive to changes in the dissipation range spectral index than the random sweeping mean free paths for both radial distances shown. Varying p appears only to alter the magnitude of the low-energy electron parallel mean free paths throughout the heliosphere, without affecting their spatial dependences.

5. COSMIC-RAY MODULATION

The results of the preceding sections are now applied to the study of the modulation of galactic CR electrons, using the QLT and ENLGC diffusion coefficients with turbulence quantities modeled using the two-component turbulence transport model of Oughton et al. (2011). A 3D, steady state CR modulation code, described by Burger et al. (2008), is applied to solve the Parker (1965) CR transport equation (TPE) for solar minimum conditions, following the approach of Engelbrecht & Burger (2013). This particular code has the advantage of being able to easily provide information as to such global quantities such as CR latitude gradients, as opposed to more recent time-dependent, stochastic TPE solvers such as those used by, e.g., Jokipii & Owens (1975), Pei et al. (2010b), and Strauss et al. (2011). The electron local interstellar spectrum here used is that of Langner et al. (2001), assuming a spherical heliosphere with a radius of 100 AU. A Parker (1958) HMF model is assumed with a magnitude at Earth chosen to be 5 nT, the tilt angle of the heliospheric current sheet is taken to be 5°, the solar wind profile assumed to be latitude dependent, and the current sheet is treated following the approach of Burger (2012). Perpendicular diffusion is assumed to be axisymmetric.

The effects of a termination shock or heliosheath are not included in the present study. This is a limitation, in that observations and numerical simulations have shown that some modulation can occur within the heliosheath (see, e.g., Caballero-Lopez et al. 2010; Burlaga et al. 2011). The exclusion of effects due to the heliosheath is done for two reasons (Engelbrecht & Burger 2013), the first of which is that the Oughton et al. (2011) was derived assuming an Alfvén speed considerably smaller than the solar wind speed, which is not the case in the heliosheath. Second, not much is observationally known for certain regarding the large-scale structure and quantities, such as the HMF, solar wind, and current sheet profiles, beyond that which has been gleaned from *Voyager* data in the small region traversed by these spacecrafts, with even less information available regarding the turbulence conditions in this region. Various results of MHD simulations for the large-scale plasma quantities have been published (see, e.g., Florinski et al. 2011) but little observational data exist that allow for an accurate assessment of the results yielded by these simulations for a large part of the region they describe.

The low-rigidity electron mean free paths, both parallel and perpendicular to the HMF, are extremely sensitive to changes in parameters pertaining to the dissipation range of the assumed slab turbulence power spectrum. This sensitivity will be investigated applying the best-fit 2D outerscale model used by Engelbrecht & Burger (2013). Comparisons will be made with solar minimum intensities reported at Earth by Moses (1987), L'Heureux & Meyer (1976), Evenson et al. (1983), Boezio et al.

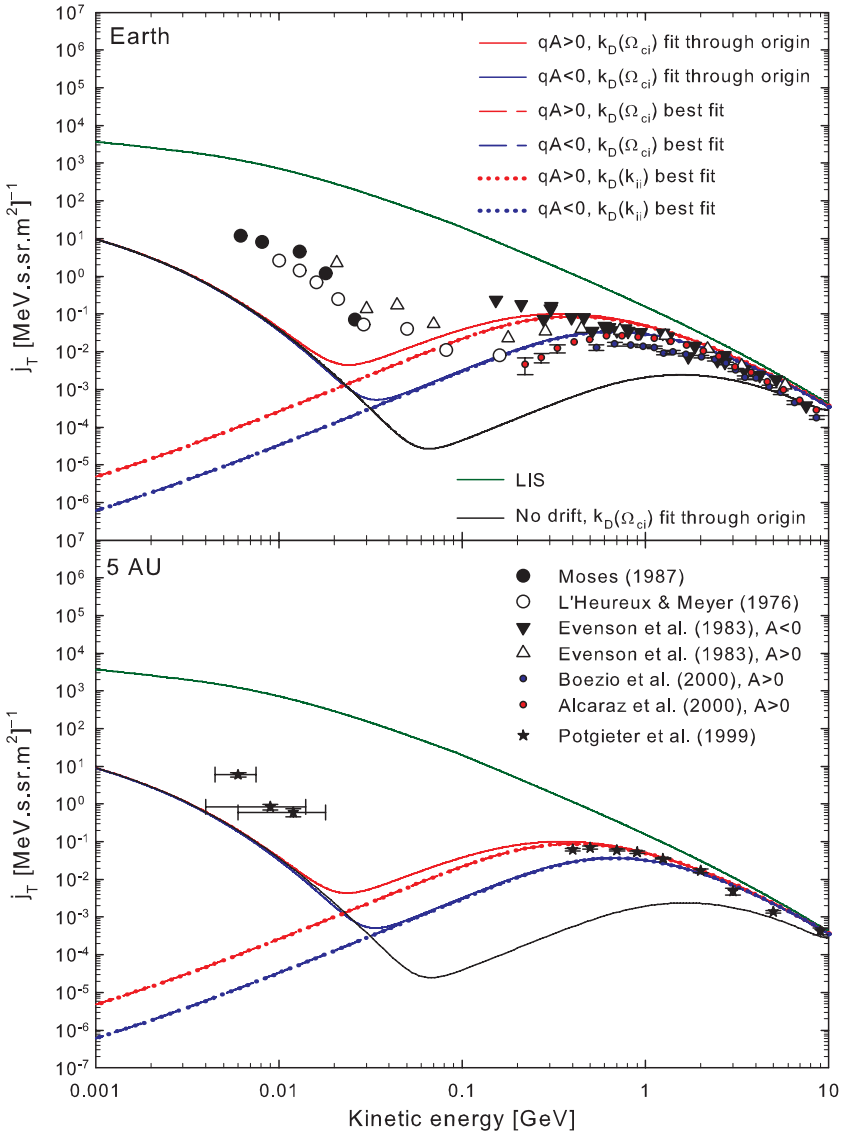

Figure 6. Galactic cosmic-ray electron intensity spectra at Earth (top panel) and at 5 AU (bottom panel), as a function of kinetic energy for various Leamon et al. (2000) models for the dissipation range spectral breakpoint wavenumber, from Engelbrecht (2013). Note that the two sets of best-fit spectra are almost identical. Spacecraft data shown are reported by Moses (1987), L'Heureux & Meyer (1976), Evenson et al. (1983), Boezio et al. (2000), Alcaraz et al. (2000), and Potgieter & Ferreira (1999).

(A color version of this figure is available in the online journal.)

(2000), and Alcaraz et al. (2000), and with intensities reported at 5 AU by Potgieter & Ferreira (1999). Intensities reported by Moses (1987) and L'Heureux & Meyer (1976), pertaining as they do to a considerable Jovian component (see also Ferreira et al. 2001a, 2001b; Ferreira 2002), are included only for the purposes of comparison as an upper limit for intensities yielded by the 3D modulation code in this study. Conclusions, however, can still be drawn as to the behavior of low-energy galactic electrons, as the total contribution of this component to the CR electron intensity at Earth has been estimated at ∼20% (Ferreira 2002). Computed latitude gradients will be compared with the data point presented by Heber et al. (2008). A reference set of dissipation range turbulence quantities is assumed as a point of departure. The reference parallel mean free path is chosen to be the random sweeping result (Equation (3)), using the Leamon et al. (2000) fit-through-origin proton gyrofrequency model for the dissipation range breakpoint wavenumber, and choosing the dissipation range spectral index to be equal to 2.6, after Smith et al. (2006). In what follows, the same 2D outerscale as that used by Engelbrecht & Burger (2013) is adopted, where $\lambda_{\rm out} = 12.5\lambda_{c,2D}$.

5.1. Effect of the Dissipation Range Breakpoint Wavenumber

Figure 6 shows galactic CR electron intensities as functions of kinetic energy at Earth and at 5 AU, for the extrapolated Leamon et al. (2000) models for the dissipation range breakpoint wavenumber k_D. There is a clear charge-sign dependence in the solutions, with intensities corresponding to $A < 0$ conditions (hence, $qA > 0$) being consistently larger than those corresponding to $A > 0$ conditions. At the highest energies shown, the choice of k_D has virtually no effect on the computed electron intensities. This is a consequence of the fact that the electron parallel mean free paths used here are essentially independent of quantities pertaining to the dissipation range on the slab turbulence power spectrum at these

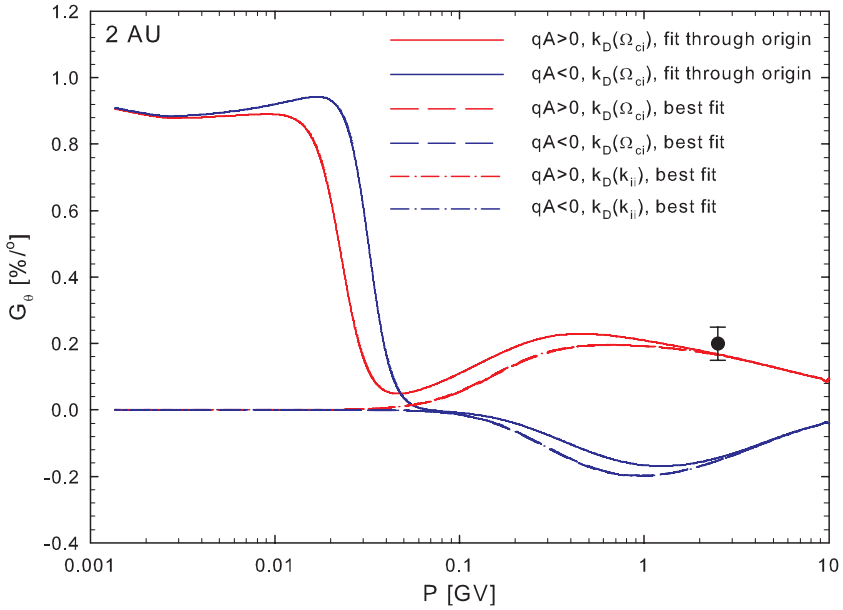

Figure 7. Galactic cosmic-ray electron latitude gradients at 2 AU, as a function of rigidity for various Leamon et al. (2000) models for the dissipation range spectral breakpoint wavenumber, from Engelbrecht (2013). Note that the two sets of best-fit latitude gradients are almost identical. Spacecraft data point shown is that reported by Heber et al. (2008).

(A color version of this figure is available in the online journal.)

energies. The intensities yielded by this approach are in relatively good agreement with the high-energy observations shown, for both magnetic polarity cycles, and at both radial distances considered.

At intermediate to low energies, however, the effects of the different models for the dissipation range breakpoint wavenumber become more readily apparent. Both best-fit models lead to spectra that are essentially identical and display a strong charge-sign dependence down to the lowest energies shown. Use of the fit-through-origin proton gyrofrequency model for k_D, however, yields intensities that show a clear increase at intermediate energies, following the trend of the observations but remaining below them, and relax toward the no-drift solution corresponding to the fit-through-origin proton gyrofrequency model shown in Figure 6, as expected when drift effects become unimportant at low energies (see, e.g., Potgieter 1996). Below ~0.1 GeV, all computed spectra display an E^2 kinetic energy dependence, a hallmark of having relaxed to the relativistic adiabatic limit (Caballero-Lopez et al. 2010). Spectra computed using the best-fit models for k_D, however, remain in this limit down to the lowest energies shown. These differences in the solutions corresponding to the various models for k_D can be understood in terms of the behavior of the parallel-mean free paths in the outer heliosphere. From Sections 3 and 4, the fit-through-origin proton gyrofrequency model yields the smallest values for k_D of the various models in the outer heliosphere, and hence the largest values for the electron parallel-mean free path at small rigidities. The best-fit models yield very similar values for k_D in this region, and consequently very similar parallel mean free paths, considerably smaller than those for the fit-through-origin proton gyrofrequency model. As the ENLGC perpendicular mean free paths here used are functions of $\lambda_\parallel$ (and are larger for larger given values of $\lambda_\parallel$, and vice versa), this reasoning applies equally to their behavior at lower rigidities, and explains the similarity of the CR intensities computed when the best-fit models for k_D are used. The charge-sign dependence seen at the lowest energies for electron intensities when the best-fit models for the dissipation range breakpoint wavenumber are used is then a direct consequence of the fact that, due to the smaller parallel and perpendicular mean free paths for these models, drift effects dominate the transport of the galactic electrons at low energies, which is clearly not the case when the fit-through-origin proton gyrofrequency model for k_D is applied.

The computed galactic electron latitude gradients, illustrated in Figure 7, appear independent of the dissipation range breakpoint wavenumber at the highest rigidities shown, for the same reason as outlined above. The signs of latitude gradients for $A > 0$ and $A < 0$ are as expected of negatively charged CRs (see, e.g., Jokipii & Thomas 1981), in that latitude gradients corresponding to $A < 0$ (i.e., $qA > 0$) are positive, and vice versa. The computed $qA > 0$ latitude gradients shown all agree, within uncertainty, with the Heber et al. (2008) data point shown. At lower rigidities, the effects of the various models for k_D can clearly be seen, with the results for the fit-through-origin proton gyrofrequency model relaxing to charge-sign independent solutions at the lowest energies shown. The latitude gradients for the best-fit models for k_D are very similar, again due to the similarity of the mean free paths yielded by these quantities. At intermediate rigidities, however, use of the best-fit models for k_D leads to somewhat smaller latitude gradients than for the case of the fit-through-origin proton-gyrofrequency model during $qA > 0$, and somewhat larger latitude gradients during $qA < 0$. This is due to the greater effects of drifts, relative to the smaller mean free paths acquired for the best-fit models for k_D. The disappearance of the latitude gradients computed for the best-fit k_D models below about 0.1 GV is a consequence of the adiabatic cooling of these CRs (Caballero-Lopez et al. 2010), and occurs when the E^2 behavior is seen in the energy spectra shown in Figure 6. At the lowest energy shown, latitude gradients again become finite for the fit-through-origin model, and the spectra in Figure 6 start to increase from the E^2 limit.

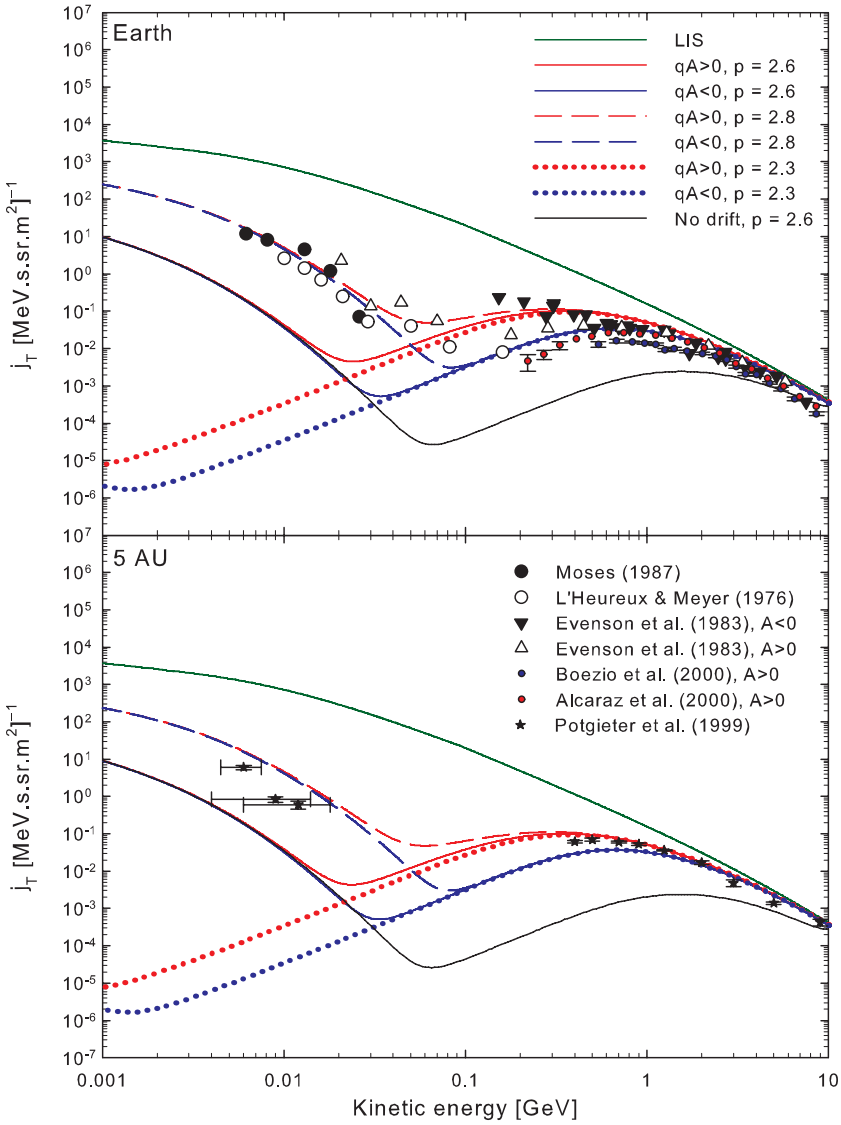

Figure 8. Galactic cosmic-ray electron intensity spectra at Earth (top panel) and at 5 AU (bottom panel), as a function of kinetic energy for various values for the dissipation range spectral index, from Engelbrecht (2013). Spacecraft data shown are reported by Moses (1987), L'Heureux & Meyer (1976), Evenson et al. (1983), Boezio et al. (2000), Alcaraz et al. (2000), and Potgieter & Ferreira (1999).

(A color version of this figure is available in the online journal.)

5.2. Effect of the Dissipation Range Spectral Index

The results of the previous subsection show that the use of the fit-through-origin proton gyrofrequency model yields galactic electron intensities in reasonable agreement with observations at high energies, and qualitative agreement at lower energies. Therefore this model for k_D is chosen as a reference model, with which the effects on CR intensities of other quantities that influence the behavior of the low-rigidity electron mean free paths will be compared. This subsection aims to illustrate the effect that varying the dissipation range spectral index, within the range $p = 2.61 \pm 0.96$ reported by Smith et al. (2006) at Earth, would have on these intensities.

Galactic electron intensities, computed assuming values of 2.3, 2.6, and 2.8 for the dissipation range spectral index, are shown as function of kinetic energy at Earth and at 5 AU in the ecliptic in Figure 8. From Section 4, an increase in p leads to a larger low-rigidity electron parallel mean free path, which, in turn, leads to a larger low-rigidity perpendicular mean free path. The effects of this are evident in Figure 8, where the smaller mean free paths implied by $p = 2.3$ lead to a drift dominated electron spectrum at both 1 AU and 5 AU. It is interesting to note that at the very lowest energies, the $p = 2.3$ solutions show the slightest indication of turning up, after displaying the relativistic adiabatic limit E^2 kinetic energy dependence seen in Figure 6. The $p = 2.8$ case yields intensities large enough to agree with the low-energy Moses (1987), L'Heureux & Meyer (1976), and Potgieter & Ferreira (1999) spacecraft data. These data are usually assumed to consist largely of Jovian electrons, and can in that light be viewed as an upper limit for the current comparison. Evenson (2011), however, argues that due to the differences in the power-law behavior of low-energy electron spectra observed by means of balloon-borne experiments with those expected of Jovian electron intensities, the galactic component at energies below 100 MeV may be the predominant one. Above about 0.1 GeV, as before, the choice of dissipation range spectral index has no effect, given the nature of the parallel mean free paths here used.

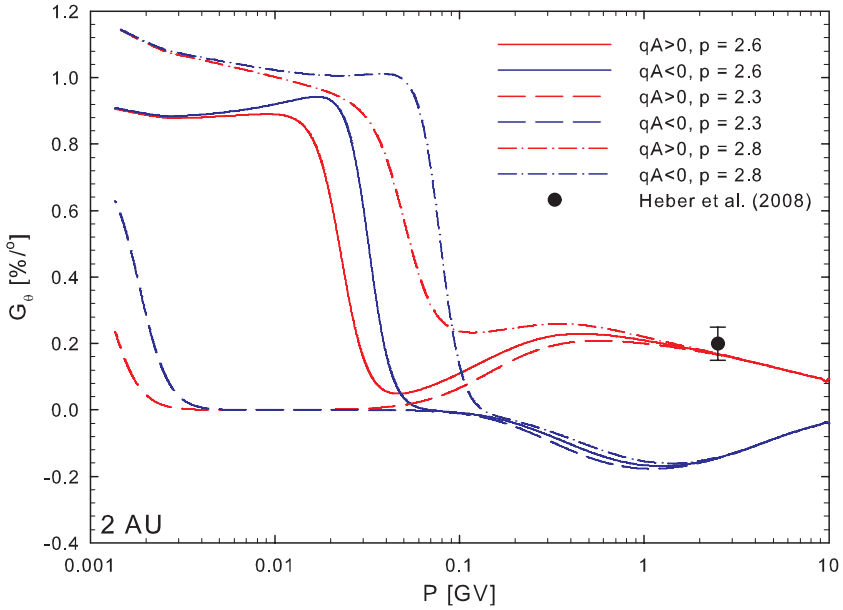

Figure 9. Galactic cosmic-ray electron latitude gradients at 2 AU as a function of rigidity for various values for the dissipation range spectral index, from Engelbrecht (2013). Spacecraft data point shown is that reported by Heber et al. (2008).

(A color version of this figure is available in the online journal.)

Figure 9 shows computed latitude gradients as function of rigidity, calculated at 2 AU for the various values here considered for the dissipation range spectral index. At lower rigidities, the $p = 2.8$ and $p = 2.6$ cases relax to no-drift values, with latitude gradients for the larger value of p being significantly larger below about 0.1 GeV. To determine at what energy a no-drift scenario occurs for the $p = 2.3$ case would require runs to lower energies, although the latitude gradients for this case do show an increase at the very lowest rigidities considered. Before this increase, however, latitude gradients for the $p = 2.3$ case vanish, due to the effects of adiabatic cooling (Caballero-Lopez et al. 2010). At the highest rigidities, varying the dissipation range spectral index has no effect on the latitude gradients, as expected.

5.3. *Effect of the Assumed Model for Dynamical Turbulence*

From Section 4, it is clear that the choice of the random sweeping or the damping model for dynamical turbulence has a significant effect on the low-rigidity electron parallel mean free paths. The effects this choice has on computed galactic electron intensities will be the subject of this subsection. Here, a random sweeping parallel mean free path expression using the fit through the origin proton-gyrofrequency model for the dissipation range breakpoint wavenumber, with a value of $p = 2.6$ for the dissipation range spectral index, will be assumed as a reference.

Figure 10 shows computed galactic electron intensities at 5 AU and at Earth for the random sweeping and damping turbulence mean free paths where $p = 2.6$, and the damping turbulence parallel mean free path where $p = 2.8$. It is immediately clear that the use of the damping turbulence mean free paths, these being consistently smaller than their random sweeping counterparts, leads to drift dominated electron intensities at lower energies. This is the case even when $p = 2.8$. This latter case, however, does show some increase at the very lowest energies shown. This is an intriguing result, in that the damping turbulence model yielding low-rigidity electron parallel mean free paths at Earth closest to the Palmer (1982) consensus range, as opposed to the random sweeping parallel mean free path that yields values considerably above this range, results in computed intensities at Earth that in no way can be construed as realistic. This highlights the potential dangers of drawing conclusions as to diffusion coefficients based on 1 AU data, and extrapolating such conclusions throughout the heliosphere. At higher energies, the choice of model for dynamical turbulence does not affect the computed CR intensities, as expected from the mean free paths presented above for the random sweeping and damping turbulence models at these energies, which are essentially identical.

6. SUMMARY AND CONCLUSIONS

This study presents a first attempt at the self-consistent application of the results yielded by a two-component turbulence-transport model to the ab initio study of galactic CR electron modulation. This was done by solving the Oughton et al. (2011) turbulence transport model for typical solar minimum heliospheric conditions such that the turbulence quantities are reasonable in agreement with spacecraft observations taken in the solar ecliptic plane in general, and with observations taken along the trajectory of *Ulysses*. These turbulence quantities were then used as inputs for chosen forms for the slab and 2D turbulence power spectra, which, in turn, were used as inputs for parallel-mean free path expressions based on the QLT results of Teufel & Schlickeiser (2003) and perpendicular mean free path expressions derived from the ENLGC theory of Shalchi (2006). To self-consistently incorporate the effects of the modeled turbulence on CR drifts, an expression for the 2D ultrascale was derived from the expression for the chosen 2D turbulence power spectrum. This spectrum was constructed, following Matthaeus et al. (2007), in such a way as to drop off at the lowest wavenumbers. This behavior, commencing at a wavenumber corresponding to what is termed in this study the 2D outerscale, is physically motivated by Matthaeus et al. (2007) and ensures a non-diverging expression for the 2D ultrascale. As the 2D outerscale is a key

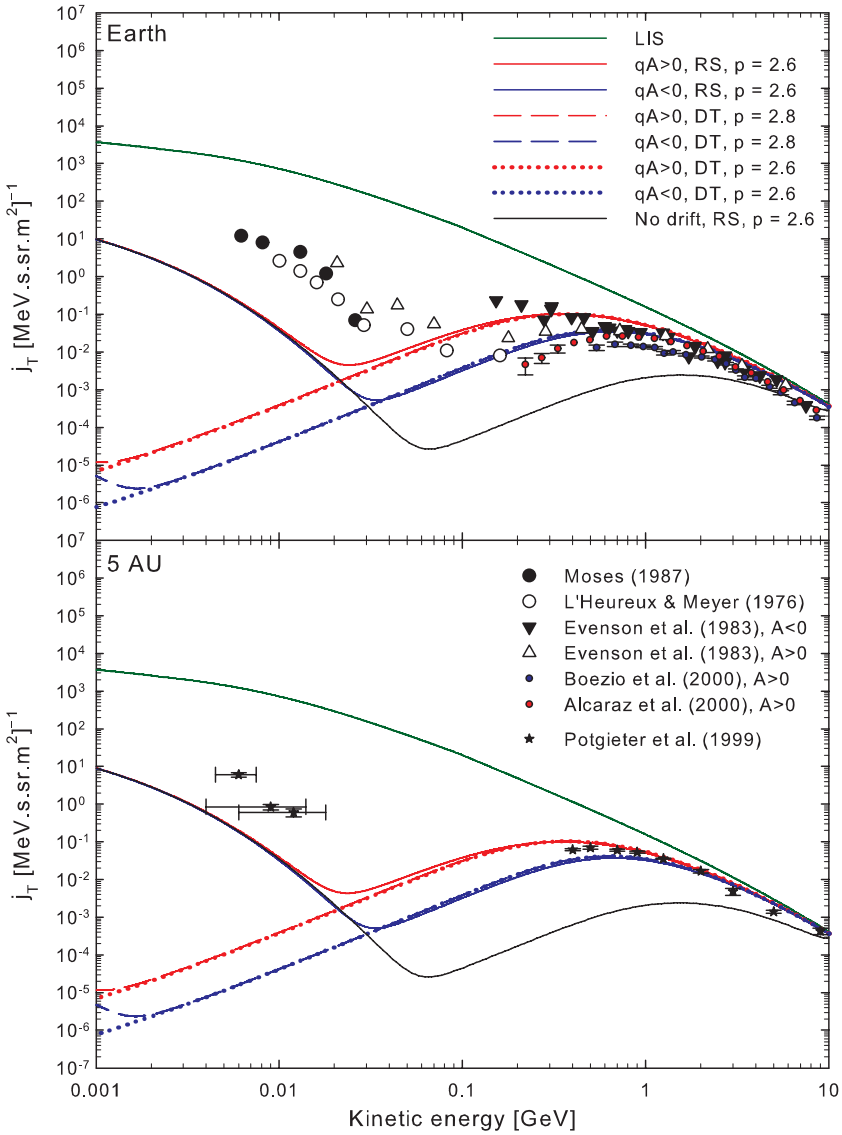

Figure 10. Galactic cosmic-ray electron intensity spectra at Earth (top panel) and at 5 AU (bottom panel), as a function of kinetic energy for parallel mean free paths acquired assuming the random sweeping (RS) and damping (DT) models for dynamical turbulence, from Engelbrecht (2013). Spacecraft data shown are reported by Moses (1987), L'Heureux & Meyer (1976), Evenson et al. (1983), Boezio et al. (2000), Alcaraz et al. (2000), and Potgieter & Ferreira (1999).
(A color version of this figure is available in the online journal.)

component of the 2D turbulence power spectrum, the perpendicular mean free paths derived using such a spectrum will also be sensitive to this quantity's behavior. The 2D ultrascale is then used in expressions for the reduced drift coefficient proposed by Burger & Visser (2010), again using the results of the turbulence transport model to describe the relevant turbulence quantities. The drift and diffusion coefficients were then used in a 3D, steady state numerical CR modulation code, assuming a relatively simple form for the 2D outerscale.

Computed galactic electron intensities were found to be extremely sensitive to even moderate changes in turbulence quantities pertaining to the dissipation range of the slab turbulence power spectrum. At higher energies, computed galactic electron differential intensities displayed no sensitivity to dissipation range parameters, and were found to be in fair agreement with spacecraft observations. Computed galactic electron latitude gradients were found to fall within the uncertainty of the single data point reported by Heber et al. (2008), displaying a high degree of sensitivity to the choices made for dissipation range parameters at low rigidities. An investigation into the effects the extrapolated Leamon et al. (2000) models for the dissipation range spectral breakpoint wavenumber would have on computed galactic electron intensities revealed that only one of these models, the fit-through-origin proton gyrofrequency model, led to intensities at lower energies in qualitative agreement with observations. The other models resulted in galactic electron spectra that displayed a clear charge-sign dependence down to the lowest energies considered, a clearly unphysical result. One model was already eliminated because it does not yield a finite dissipation range above the solar poles. Varying the dissipation range spectral index within the uncertainties of the Smith et al. (2006) observations also had a significant effect on low-energy electron differential intensity spectra, with the solutions computed using a small value ($p = 2.3$) for this quantity exhibiting charge-sign dependences contrary to observations, while the use of a large ($p = 2.8$) value led to intensities so large as to agree with observations believed to contain a large Jovian component, such as those reported by Moses (1987). The

aforementioned results were obtained assuming electron parallel mean free paths derived using the random sweeping model for dynamical turbulence. Differential intensities computed assuming mean free paths derived using the damping model of dynamical turbulence displayed a clear charge-sign dependence at lower energies, regardless of what was assumed for the dissipation range spectral index. The underlying pattern in these low-energy electron results is that dissipation range turbulence quantities need be chosen very specifically so as to compute realistic galactic electron intensities. More specifically, the ab initio model is extremely sensitive to the behavior of the low-energy parallel mean free paths in the outer heliosphere. A dissipation range turbulence quantity that results in a too-small parallel mean free path will lead to a scenario where the effects of drift dominate the effects of diffusion in the outer heliosphere, leading to charge-sign dependent differential intensities at Earth. These results again raise the possibility that it may be possible to use CR observations at Earth as a diagnostic from which conclusions may be drawn as to the global behavior of some turbulence quantities in general, or at the least on the behavior of turbulence quantities pertinent to the dissipation range of the turbulence power spectrum.

To conclude, an ab initio treatment of diffusion and drift, incorporating in as self-consistent a way possible the effects of turbulence as described by a two-component turbulence-transport model, which is set in such a way as to yield results in reasonable to good agreement with spacecraft observations of turbulence quantities, can yield computed CR intensities in reasonably good agreement with multiple sets of spacecraft observations, and for different CR species when the results of Engelbrecht & Burger (2013) are taken into account.

N.E.E. thanks Sean Oughton and John Bieber for helpful discussions. The financial assistance of the National Research Foundation (NRF) toward this research is hereby acknowledged. The opinions expressed and conclusions arrived at are those of the authors and are not necessarily to be attributed to the NRF.

REFERENCES

Alcaraz, J., Alpat, B., Ambrosi, G., et al. 2000, PhLB, 484, 10
Alexandrova, O., Carbone, V., Veltri, P., & Sorriso-Valvo, L. 2008, ApJ, 674, 1153
Bieber, J. W., & Matthaeus, W. H. 1997, ApJ, 485, 655
Bieber, J. W., Matthaeus, W. H., Smith, C. W., et al. 1994, ApJ, 420, 294
Bieber, J. W., Smith, C. W., & Matthaeus, W. H. 1988, ApJ, 334, 470
Boezio, M., Carlson, P., Francke, T., et al. 2000, ApJ, 532, 653
Breech, B., Matthaeus, W. H., Minnie, J., et al. 2008, JGR, 113, 8105
Bruno, R., & Carbone, V. 2005, LRSP, 2, 4
Burger, R. A. 2012, ApJ, 760, 60
Burger, R. A., Krüger, T. P. J., Hitge, M., & Engelbrecht, N. E. 2008, ApJ, 674, 511
Burger, R. A., & Visser, D. J. 2010, ApJ, 725, 1366
Burlaga, L. F., Ness, N. F., Stone, E., & McDonald, F. B. 2011, JGR, 116, 12104
Caballero-Lopez, R. A., Moraal, H., & McDonald, F. B. 2010, ApJ, 725, 121
Carbone, V. 2012, SSRv, 172, 343
Della Torre, S., Bobik, P., Boschini, M. J., et al. 2012, AdSpR, 49, 1587
Dröge, W. 1994, ApJS, 90, 567
Dröge, W. 2000, ApJ, 537, 1073
Dröge, W. 2003, ApJ, 589, 1027
Engelbrecht, N. E. 2013, PhD thesis, North-West Univ.
Engelbrecht, N. E., & Burger, R. A. 2010, AdSpR, 45, 1015
Engelbrecht, N. E., & Burger, R. A. 2013, ApJ, 772, 46
Erdös, G, & Balogh, A. 2005, AdSpR, 35, 625
Evenson, P. 2011, in Proc. International Cosmic Ray Conference, Vol. 11, SH3-SH4: Solar and Heliospheric Phenomena (Beijing: IUPAP), 54
Evenson, P., Garcia-Munoz, M., Meyer, P., Pyle, K. R., & Simpson, J. A. 1983, ApJL, 275, L15
Ferreira, S. E. S. 2002, PhD thesis, Potchefstroomse Universiteit vir Christelike Hoër Onderwys
Ferreira, S. E. S., Potgieter, M. S., Burger, R. A., Heber, B., & Fichtner, H. 2001a, JGR, 106, 24979
Ferreira, S. E. S., Potgieter, M. S., Burger, R. A., et al. 2001b, JGR, 106, 29313
Florinski, V., Ferreira, S. E. S., & Pogorelov, N. V. 2011, SSRv, 176, 147
Goldstein, M. L., Roberts, D. A., & Fitch, C. A. 1994, JGR, 99, 11519
Hamilton, K., Smith, C. W., Vasquez, B. J., & Leamon, R. J. 2008, JGR, 113, 1106
Heber, B., Gieseler, J., Dunzlaff, P., et al. 2008, ApJ, 689, 1443
Howes, G. G., Cowley, S. C., Dorland, W., et al. 2008, JGR, 113, 5103
Jokipii, J. R. 1966, ApJ, 146, 480
Jokipii, J. R., & Owens, A. J. 1975, JGR, 80, 1209
Jokipii, J. R., & Thomas, B. 1981, ApJ, 243, 1115
Langner, U. W., de Jager, O. C., & Potgieter, M. S. 2001, AdSpR, 27, 517
Leamon, R. J., Matthaeus, W. H., Smith, C. W., et al. 2000, ApJ, 537, 1054
Leamon, R. J., Smith, C. W., & Ness, N. F. 1998a, GeoRL, 25, 2505
Leamon, R. J., Smith, C. W., Ness, N. F., Matthaeus, W. H., & Wong, H. K. 1998b, JGR, 103, 4775
L'Heureux, J., & Meyer, P. 1976, ApJ, 209, 955
Maccione, L. 2013, PhRvL, 110, 081101
Marsch, E. 2006, LRSP, 3, 1
Matthaeus, W. H., Bieber, J. W., Ruffolo, D., Chuychai, P., & Minnie, J. 2007, ApJ, 667, 956
Matthaeus, W. H., Gray, P. C., Pontius, D. H., Jr., & Bieber, J. W. 1995, PhRvL, 75, 2136
Matthaeus, W. H., Qin, G., Bieber, J. W., & Zank, G. P. 2003, ApJL, 590, L53
Matthaeus, W. H., & Velli, M. 2011, SSRv, 160, 145
Matthaeus, W. H., Zank, G. P., Smith, C. W., & Oughton, S. 1999, PhRvL, 82, 3444
McComas, D. J., Barraclough, B. L., Funsten, H. O., et al. 2000, JGR, 105, 10419
Minnie, J., Bieber, J. W., Matthaeus, W. H., & Burger, R. A. 2007a, ApJ, 663, 1049
Minnie, J., Bieber, J. W., Matthaeus, W. H., & Burger, R. A. 2007b, ApJ, 670, 1149
Moses, D. 1987, ApJ, 313, 471
Oughton, S., Matthaeus, W. H., & Dmitruk, P. 2006, PhPl, 13, 042306
Oughton, S., Matthaeus, W. H., Smith, C. W., Bieber, J. W., & Isenberg, P. A. 2011, JGR, 116, 8105
Palmer, I. D. 1982, RvGSP, 20, 335
Parker, E. N. 1958, ApJ, 128, 664
Parker, E. N. 1965, P&SS, 13, 9
Pei, C., Bieber, J. W., Breech, B., et al. 2010a, JGR, 115, 3103
Pei, C., Bieber, J. W., Burger, R. A., & Clem, J. 2010b, JGR, 115, 12107
Potgieter, M. S. 1996, JGR, 101, 24411
Potgieter, M. S., & Ferreira, S. E. S. 1999, AdSpR, 23, 463
Potgieter, M. S., & Nndanganeni, R. R. 2013, Ap&SS, 345, 33
Shalchi, A. 2006, A&A, 453, L43
Shalchi, A. 2009, Nonlinear Cosmic Ray Diffusion Theories (Berlin: Springer-Verlag)
Shalchi, A., Bieber, J. W., & Matthaeus, W. H. 2004a, ApJ, 604, 675
Shalchi, A., Bieber, J. W., & Matthaeus, W. H. 2004b, ApJ, 604, 805
Shalchi, A., Bieber, J. W., Matthaeus, W. H., & Schlickeiser, R. 2006, ApJ, 642, 230
Shalchi, A., & Schlickeiser, R. 2004, ApJ, 604, 861
Smith, C. W., Bieber, J. W., & Matthaeus, W. H. 1990, ApJ, 363, 283
Smith, C. W., Hamilton, K., Vasquez, B. J., & Leamon, R. J. 2006, ApJL, 645, L85
Smith, C. W., Vasquez, B. J., & Hollweg, J. V. 2012, ApJ, 745, 8
Stawicki, O., Gary, S. P., & Li, H. 2001, JGR, 106, 8273
Strauss, R. D., Potgieter, M. S., Büsching, I., & Kopp, A. 2011, ApJ, 735, 83
Teufel, A., & Schlickeiser, R. 2003, A&A, 397, 15
Tu, C. Y., & Marsch, E. 1993, JGR, 98, 1257